980 nm QW micro-lasers with ultra-low threshold

Qi Lin,[1,2] Ying Xue,[1,2] Jie Huang,[1] Wen Gu,[1] and Kei May Lau[1 *]

[1]*Division of Emerging Interdisciplinary Area, Hong Kong University of Science and Technology, Clear Water Bay, Kowloon, Hong Kong*

[2]*These authors contributed equally to this work*

**eekmlau@ust.hk*

***Abstract*—980 nm lasers, critical for pumping erbium-doped fiber amplifiers (EDFAs) in optical communication systems, are also gaining traction in emerging biological applications. To achieve dense integration and low power consumption, we developed high-performance 980 nm micro-lasers on both GaAs and Si substrates. This work combines quantum well (QW) active regions with micro-cavities, including micro-ring lasers (MRLs) and micro-disk lasers (MDLs) with optimized metal designs. Advanced passivation techniques were applied to suppress sidewall surface recombination, significantly improving laser performance. Here, we report the first room-temperature continuous-wave (CW) operation of electrically pumped QW micro-lasers at 980 nm. Achieving a low CW threshold current of 2.4 mA and operation at elevated temperatures exceeding 95 °C (measurement setup limit), the lasers also demonstrated sub-milliamp thresholds in pulsed mode. The optimized micro-lasers exhibited little degradation over six months of storage, showing stability. We discuss the limitations of QW micro-lasers, corresponding solutions, and the underlying physics. With their small footprint, low thresholds, and stable performance under preliminary tests, QW micro-lasers are promising on-chip light sources for dense photonic circuit integration.**

***Index Terms*—980nm, quantum well, micro cavities, passivation, stability**

I. INTRODUCTION

The increasing demand for data movement in cutting-edge technologies is pushing the electronic device scaling, as dictated by Moore's law, toward its physical limits. Photonic integrated circuits (PICs) have emerged as a promising solution to address this bottleneck, requiring compact light sources with low power consumption and a small footprint [1-2]. Micro-lasers, supporting whispering gallery modes (WGMs) at the resonator periphery, are ideal candidates for such light sources due to their high efficiency [3-4]. Featured with high-quality (Q) cavities and small mode volumes, micro-ring lasers (MRLs) exhibit low thresholds and high direct modulation speeds, making them particularly advantageous compared to other cavity designs [5-7]. However, as the resonator size reduces to tens of microns, non-radiative surface recombination at the micro-resonator sidewalls becomes a major challenge, leading to significant optical loss. To meet the demands of high-gain and high-speed applications, quantum wells (QWs) are often adopted as the active region [8]. Nevertheless, QW lasers are more sensitive to sidewall roughness due to their longer carrier diffusion lengths, resulting in higher recombination rates, increased thresholds, reduced output power, and diminished reliability [9-10].

In our previous study, we have reported 980 nm InGaAs/GaAs/GaAsP QW Fabry-Perot (FP) laser diodes with continuous-wave (CW) threshold currents of approximately 50 mA [11-12]. To achieve a compact, reliable 980 nm laser source suitable for miniaturization while minimizing sensitivity to non-radiative recombination at the resonator sidewalls, optimizing the laser structure and employing effective passivation techniques are essential. MDLs with full disk metal contacts, without the inner sidewall of the cavity, could relatively suppress the non-radiative recombination compared to MRLs. However, the inactive central region of the cavity increases the lasing threshold [13]. In this work, we propose a novel design: micro-disk lasers with ring-shape metal (MDRMs), combining the MD cavity with only one etched sidewall, and a ring-shape metal for minimum loss induced by the inactive center region. Additionally, atomic layer deposition (ALD) was employed for surface passivation to reduce Ga-O bonds at the etched sidewalls [14-16], thereby improving the device performance in terms of output power, lasing threshold, and reliability. We compared the performance of electrically pumped QW micro-ring lasers with and without the Al_2O_3 passivation layer.

In this study, WGM cavities with vertical and smooth sidewalls were fabricated and doubly passivated with Al_2O_3 and SiO_2 layers to achieve strong optical confinement and low scattering losses. We demonstrated room-temperature (RT) sub-milliamp threshold operation of 980 nm QW micro-cavity lasers. In CW mode, the lowest threshold current of 2.4 mA was achieved on devices with a 25 μm radius on a GaAs substrate. The lasers exhibited stable operation at elevated temperatures exceeding 95 °C (the measurement setup limit), with a large characteristic temperature of 214.6 K. Furthermore, we successfully realized 980 nm micro-lasers on GaAs/Si template with a low threshold current density of 1.16 kA/cm^2. The high-performance micro-lasers on GaAs/Si template paves the way for monolithic integration of high-performance III-V lasers with silicon photonic circuits.

This article has been accepted for publication in IEEE Journal of Selected Topics in Quantum Electronics. This is the author's version which has not been fully edited and content may change prior to final publication. Citation information: DOI 10.1109/JSTQE.2025.3573291

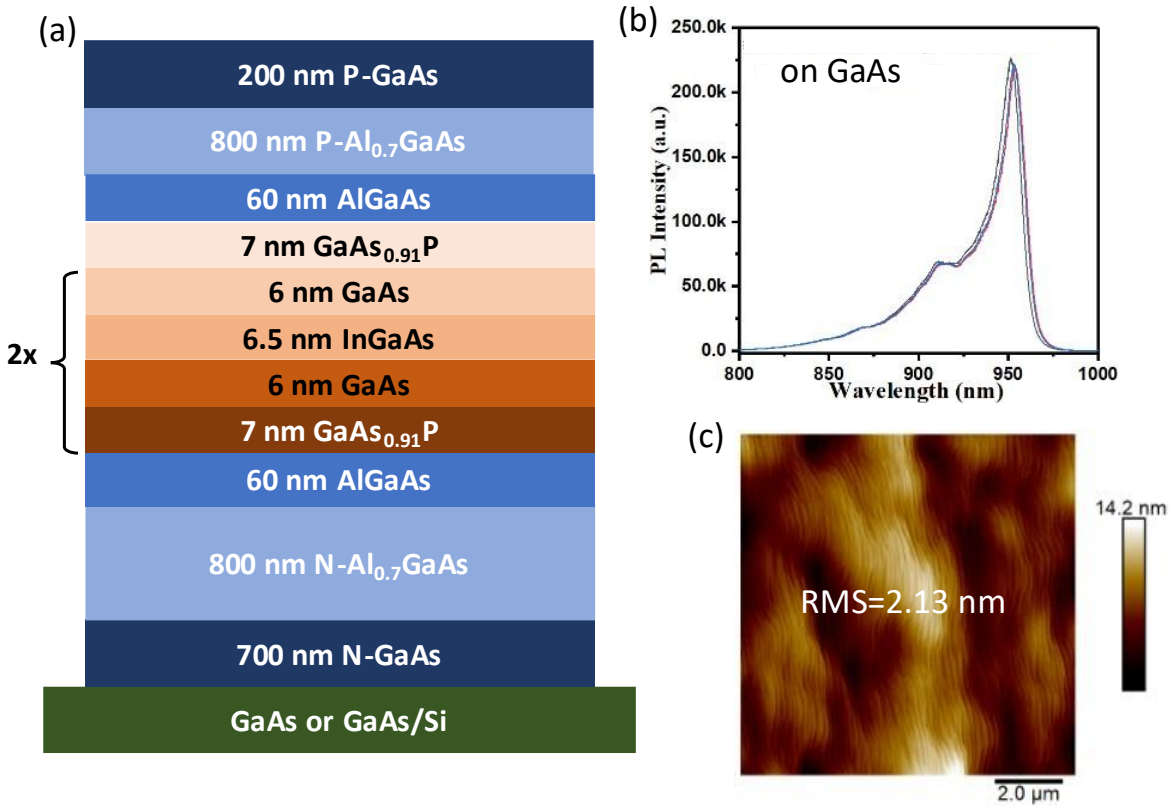

Figure 1. (a) Schematic of the 980nm InGaAs/GaAs/GaAsP QW laser grown on native GaAs and GaAs/Si template; (b) RT μPL spectra of the InGaAs/GaAs/GaAsP QW grown on GaAs; (d) AFM images of the electrically pumped InGaAs/GaAs/GaAsP QW laser.

II. Experiment

The electrically pumped InGaAs/GaAs/GaAsP QW lasers were grown on native GaAs substrate and CMOS-compatible nominal (001) Si by MOCVD. The GaAs-on-planar Si (GaAs/Si) templates and the laser structure were grown in an AIXTRON CCS system and AIXTRON 200/4 system, respectively. The schematic of the electrically pumped QW laser structure is delineated in Fig. 1(a). Strain-compensated InGaAs/GaAs/GaAsP QW structure was utilized as the active region. The detailed growth information of the QW lasers and GaAs/Si templates has been reported in our previous publications [11-12]. Fig. 1(b) shows the RT micro-photoluminescence (μPL) spectra of the InGaAs/GaAs/GaAsP QWs on GaAs without cladding and contact layer, excited by a CW 514 nm laser, exhibiting peak wavelength of 956 nm. The 10 × 10 μm^2 atomic force microscopy (AFM) image of the QW laser, as shown in Fig. 1(c), displays a root mean square (RMS) value of 2.13 nm.

The as-grown sample was then fabricated into micro-lasers, specifically micro-disk lasers (MDL) and micro-ring lasers (MRL). MRLs offer superior optical confinement compared to micro-disk lasers. However, The MRLs are highly sensitive to the smoothness of both the inner and outer sidewalls, especially for device with small radius and QW active region. Therefore, we combined a micro-disk resonator with only etched outer sidewall and a ring-shaped metal for carrier injection where the WGMs are to mitigate the limitations of MRLs. The 3D and cross-sectional schematics of the three fabricated laser structures without pad deposition are shown in Figure 2 (a)-(f). These lasers were defined by conventional photolithography, dry etching and metallization steps. Ge/Au/Ni/Au was deposited as n-metals. Passivation was then carried out in two ways: first depositing 10 nm of Al_2O_3 using atomic layer deposition (ALD), followed by 550 nm of SiO_2 using plasma-enhanced chemical vapor deposition (PECVD), or solely PECVD SiO_2. After passivation and contact hole opening, Ti/Pt/Au was deposited as p-metals. The 52°-titled view scanning electron microscopy (SEM) images of micro-lasers and zoom-in sidewall observed after metal deposition, are displayed in Fig. 2 (g)-(i), illustrating smooth sidewalls for low scattering loss.

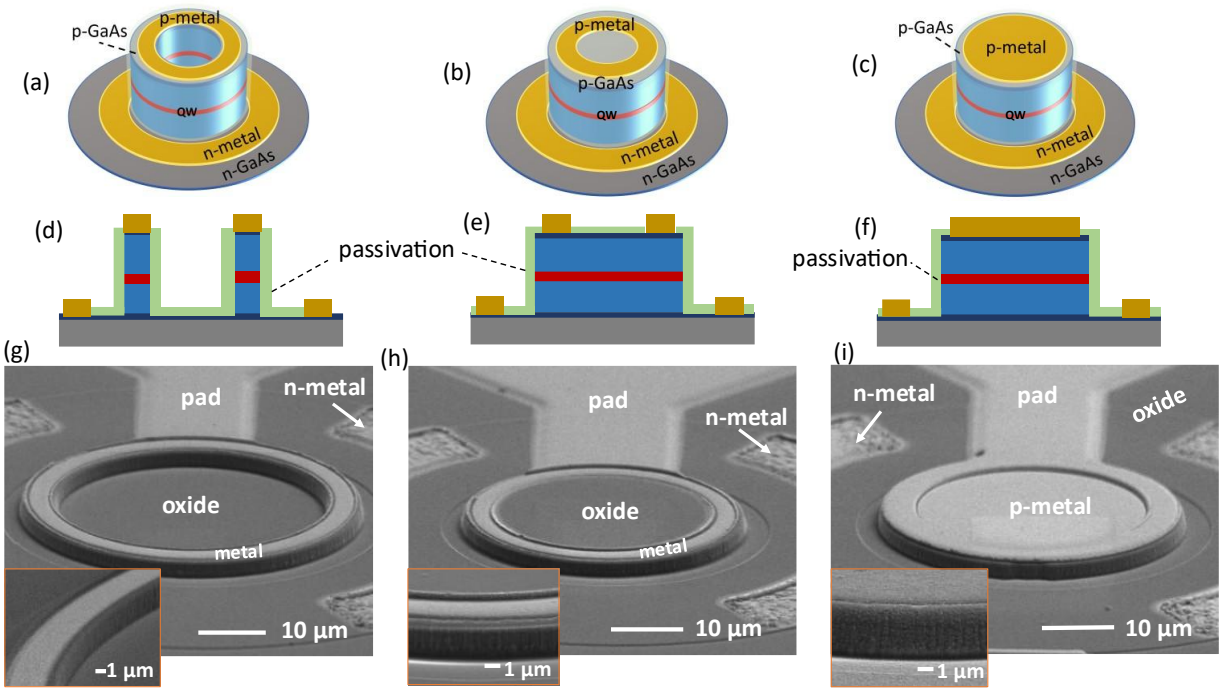

Figure 2. 3D schematics of (a) MRL, (b) MDRM and (c) MDL. (d)(e)(f) the corresponding cross-section schematic and (g)(h)(i) SEM images of the fabricated lasers. Inset: zoom-in image of corresponding sidewalls.

III. Results and Discussion

The fabricated lasers were characterized on a heatsink with a temperature controller and electrically driven by a current source in CW mode. To measure the output power, radiation out-coupling from the top of the micro-laser cavity was collected using a lensed fiber. It is worth noting that the estimated azimuthal light-radiation-collection angle for this geometry was approximately 40°. However, due to the angular directivity pattern of radiation and the limited aperture of the fiber, the presented optical power magnitude is underestimated. Figure 3 shows the lowest threshold current obtained on these three laser structures passivated by 10 nm Al_2O_3 and 550 nm SiO_2 layer. In Fig. 3(a), the light-current (*L-I*) curve of a MRL with an outer-ring radius of 15 µm and a ring width of 4 µm on the GaAs substrate was plotted, achieving CW threshold of 4 mA and output power around 3.5 µW. The spectrum measured in pulse mode, as shown in the inset of Fig. 3(a), illustrates its lasing behavior at 3 mA with a distinct lasing mode at 972 nm. The 25 µm-radius MDRM exhibits a low CW-threshold current of 2.4 mA and sub-milliampere threshold in pulsed mode, as shown in Fig.3 (b). A dominant mode is observed at 979 nm below 1 mA, and the distinction ratio was about 26 dB. The corresponding CW-threshold current density J_{th} has an ultralow value of 122 A/cm^2, which indicates excellent nonradiative recombination suppression at the deeply etched sidewalls of our QW MDLs. The 5 µm-radius MDL shows a low threshold of 4 mA in CW mode and a clear lasing peak at 982 nm below 3 mA in pulsed mode, as shown in Fig.3 (c).

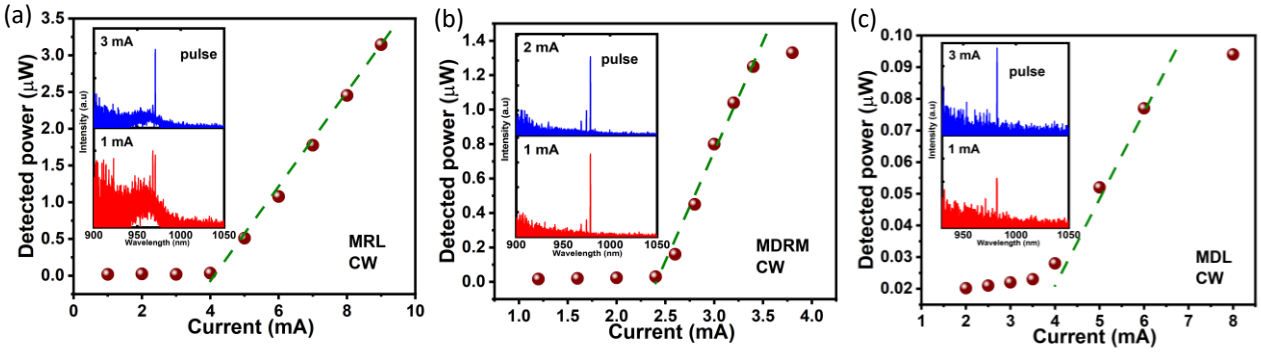

Figure 3. L-I curves with lowest threshold in CW mode of (a) 15 µm-radius MRL, (b) 25 µm-radius MDRM and (c) 5 µm-radius MDL. Inset: corresponding emission spectra at progressively increased currents of the lasers measured at 20 °C in pulse mode.

Figure 4(a) compares the *L-I* curves of MDRMs and MRLs with a 25 μm radius in CW mode. The threshold current is significantly reduced from 7 mA to 2.4 mA when using MDRMs, representing a remarkable 70% improvement. However, it is important to note that the fiber detection efficiency differs between ring and disk cavities (several times lower for MDRMs), making a direct comparison of output power impractical. Figure 4(b) depicts a plot of the average threshold current versus the outer radius of MRLs and MDRMs. As the laser radius decreases, the threshold current decreases as well, reaching 6 mA for MDRMs and 8.25 mA for MRLs. This threshold reduction highlights the suppression of nonradiative sidewall recombination in MDRMs. The difference between MRLs and MDRMs increases with the decrease of laser size as the sidewall recombination becomes significant with the shrinkage of laser size. The reduced variation in larger micro-lasers indicates that smaller-diameter lasers are more sensitive to sidewall roughness. This sensitivity arises because the optical modes are pushed closer to the cavity perimeter in smaller devices [17]. To further analyze the impact of non-radiative recombination on MRLs and MDRMs, the threshold current densities J_{th} are summarized for MRLs and MDRMs in Fig.4 (c). Larger cavities exhibit higher net gain and thus lower threshold current densities [18]. The lowest value of J_{th} is 49 A/cm^2, obtained on an 80 μm-diameter QW micro-disk laser, which is even lower than those of telecom quantum dot (QD) lasers [19-20]. The relationship between threshold current (I_{th}) and threshold current density (J_{th}) with the micro-disk laser diameter (d) is described using the following expression [21]:

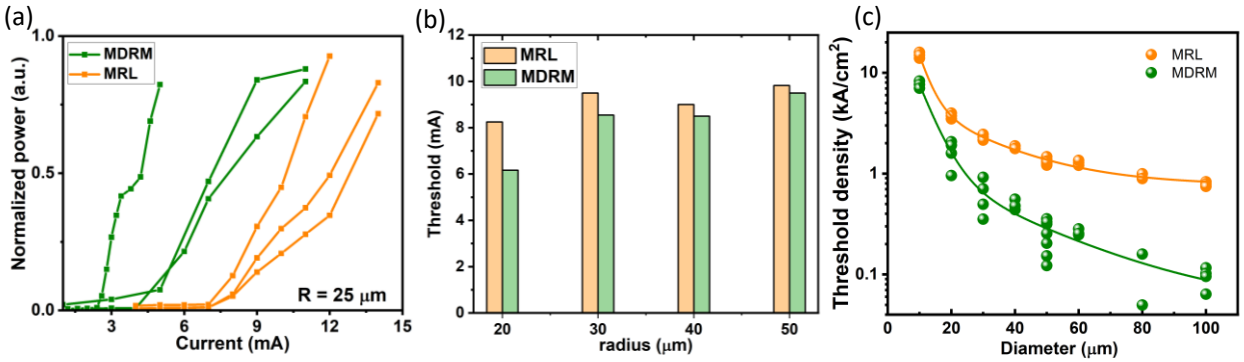

Figure 4. (a) Representative L-I curves of QW MRLs and MDRMs with 25 μm radius in CW mode; (b) Average threshold current comparison of MRLs and MDRMs with 20-50 μm radius; (c) Summary of threshold current density of MRLs and MDRMs with various cavity diameters. Solid lines are binomial approximations.

$$I_{th} = \frac{\pi d^2}{4} J_2 + \pi d j_1 \quad (1)$$

$$J_{th} \equiv \frac{I_{th}}{\frac{\pi d^2}{4}} = J_2 + \frac{4 j_1}{d} \quad (2)$$

This form of the Taylor series expansion includes two coefficients: J_2, which is associated with the recombination current in the active region, and j_1, which represents non-radiative recombination at the etched sidewall. For MRLs, the ring width is approximately 4 μm for different outer diameters (from 30 μm to 100 μm), and the lasing mode is concentrated near the outer sidewall [1]. Thus, we primarily consider non-radiative recombination at the outer sidewall of the MRLs. In Eq. (1), the d for first part will be the difference of inner and outer radius, while in the second part for surface current counting, it will refer only to the outer radius. Fitting the experimental data, the coefficients were extrapolated to

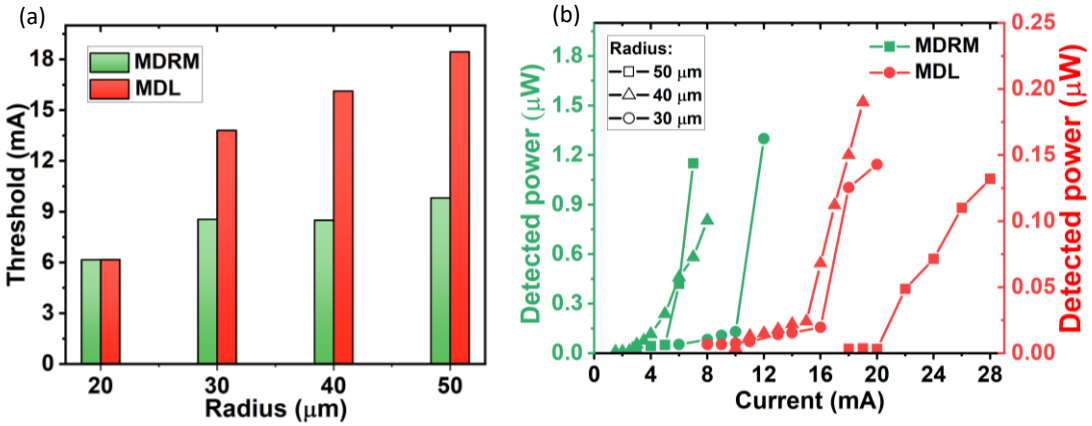

Figure 5. (a) Average threshold current comparison of MDRMs and MDLs with 20-50 μm radius; (b) Representative L-I curves of QW MDRMs and MDLs with 30/40/50 μm radius in CW mode.

This article has been accepted for publication in IEEE Journal of Selected Topics in Quantum Electronics. This is the author's version which has not been fully edited and content may change prior to final publication. Citation information: DOI 10.1109/JSTQE.2025.3573291

be J_2 = 415 A/cm^2, j_1 = 0.51 A/cm for MDRMs and J_2 = 400 A/cm^2, j_1 = 1.375 A/cm for MRLs. The j_1 value of MRL is more than twice that of MDRMs, corresponding to more sidewalls and optical modes pushed closer to sidewalls in MRLs. Meanwhile, the comparable J_2 values reflect the use of the same as-grown sample. The low j_1 of MDRM outperforms the reported QW laser on GaAs substrates [20] and is even comparable with QD lasers [22], despite the longer diffusion length of QW [23].

In Fig.5(a), the average threshold current of MDRMs and MDLs versus the disk radius is plotted. With increasing disk radius, the difference between two laser structures becomes more pronounced as the carrier injection manipulated by metal design is more obvious due to lager area difference. Specifically, as the laser diameter expands from 20 μm to 50 μm, the ratio between the radius of p-type metal and the cavity (R_{pc}) minimizes from 12.5% to 0.7%. This trend reveals that for larger-size MDRMs, reduced R_{pc} could enable more efficient manipulation of carrier injection and thus enhance the spatial overlap between carrier injection region and the optical modes. Therefore, for large-diameter MDRMs, higher internal quantum efficiency results in lower threshold current compared to MDLs. The representative *L-I* curves of two types of disk lasers with various radii are presented in Fig.5 (b). The threshold current of 40 μm disk laser is reduced from 15 mA to 4.2 mA, a 70% improvement, while the detected power of MDRMs is around 6 times of MDLs.

The thermal stability of lasers is of great importance for practical application. Temperature-dependent spectra measurements were performed to examine the high-temperature performance of MDRMs and MRLs. The natural logarithm of threshold versus temperature is plotted for MRL and MDRM with the same cavity-radius of 15 μm in Figs. 6(a)-(b). Both the lasers can lase above 95 °C, which is the limitation of the measurement setup. Using $\frac{I_{th}(T_2)}{I_{th}(T_1)} = exp(\frac{T_2-T_1}{T_0})$, the characteristic temperature of T_0 = 88.7 K and T_0 = 97.3 K can be extracted for the MRL and MDL, respectively. To further evaluate the temperature characteristics of these two laser structures and minimize thermal effects caused by CW injection current, Fig. 6(c) displays the temperature dependence of the laser modes at a fixed injection current in the pulsed mode. With increasing temperature, the lasing wavelengths of the MDRM and the MRL slightly shift by ~0.0826 nm/°C and 0.3546 nm/°C. The larger T_0 proves the QW MDRMs have better heat dissipation with improved extraction of heat from the active region [19], while the lower $d\lambda/dT$ demonstrates the lower temperature sensitivity of MDRMs due to its reduced non-radiative recombination rate.

After the micro-ring cavity definition, surface states form on the un-passivated cavity, acting as non-radiative recombination centers. These centers pin the Fermi level at the resonator surface, degrading laser performance by increasing the threshold current and shortening device lifetimes [24-25]. To minimize the non-radiative recombination on the cavity surface, surface passivation is essential. For electrically pumped lasers with top-top contact configurations, a thick passivation layer could diminish the loss caused by the metal. In this work, a thin layer of Al_2O_3 deposited by ALD was adopted before thick PECVD SiO_2 passivation layer to achieve effective passivation. Figure 7(a) summarizes the statistical thresholds of MRLs with different passivation: 10 nm Al_2O_3 before 550 nm SiO_2 and 550 nm SiO_2 alone. The MRLs with Al_2O_3/SiO_2 passivation shows lower thresholds compared to those with only SiO_2 layer, across various device dimensions (radii ranging from 5 μm to 50 μm). The MRLs with Al_2O_3 and SiO_2 passivation also demonstrate larger detected output power, as shown in representative *L-I* curves of 25 μm MRLs in Fig.7(b). To confirm the suppression of nonradiative sidewall recombination effects of the Al_2O_3/SiO_2 passivation, Eq. (2) was adopted to fit the experimental data, as presented in Fig.7 (c). The extracted coefficient j_1 = 1.89 A/cm for MRLs with only SiO2 passivation is higher than j1 = 1.375 A/cm A/cm for MRLs with the additional Al_2O_3 layer. The atomic layer-by-layer deposition process, utilizing TMA precursors, aids in combating ion-bombardment effects and native oxide formation on the etched sidewalls. This deposition method chemically reduces and substitutes the native oxide with Al_2O_3, thereby assisting in unpinning the Fermi level and decreasing interface trap density [26]. As a result, the overall impact is a reduction in sidewall non-radiative recombination, leading to improved device performance and reliability.

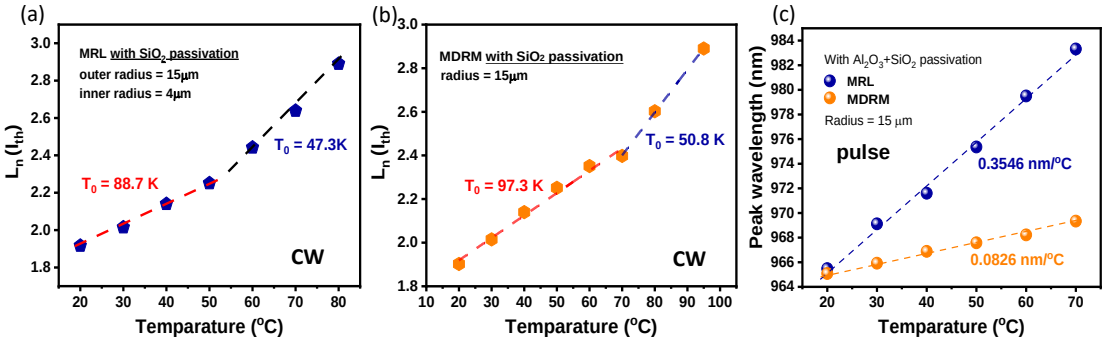

Figure 6. Characteristic temperature of electrically pumped QW (a) MRL and (b) MDRM with 15 μm radius in CW mode; (c) Lasing wavelength as a function of injection current for the primary lasing modes of the MRL and MDRM in pulse mode.

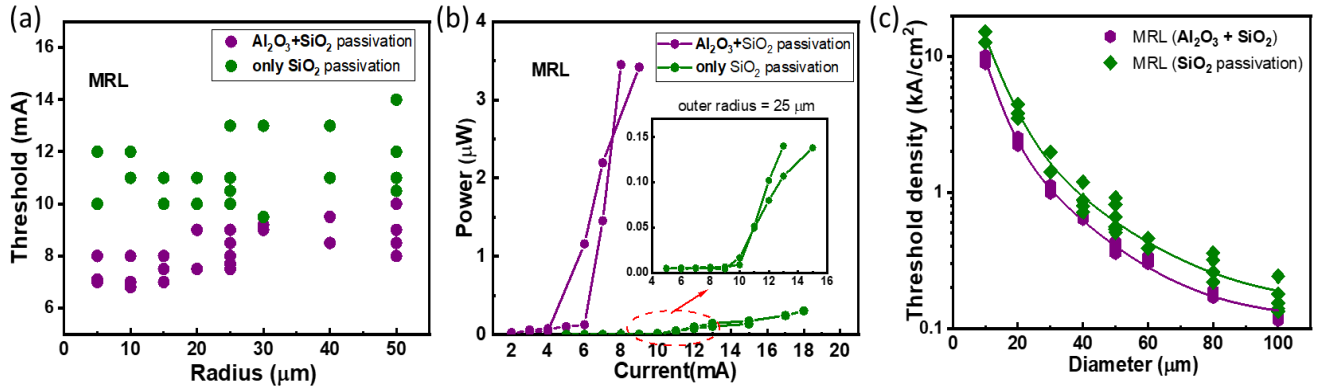

Figure 7. (a) CW threshold current distribution of different-radii MRLs with two types of passivation; (b) Representative L-I curves of MRLs with 25 μm radius with and without Al_2O_3 layer before SiO_2 layer; Inset: the zoom in L-I curves of MRLs with only SiO_2 passivation; (c) Summary and fitting of threshold density of MRLs with various cavity diameters.

High-temperature operation of MRLs was also performed to investigate the impact of the Al_2O_3 layer. As shown in Fig. 8(a)-(b), two 15 μm MRLs demonstrate their highest operating temperature up to 95 °C, the limit of the measurement setup. However, during the high-temperature operation, those lasers with only SiO_2 passivation were observed easily to burn down while the devices with Al_2O_3 and SiO_2 still could continue their lasing behavior to 95 °C. The MRL with Al_2O_3 and SiO_2 passivation achieves a high T_0 of 214.6 K in the range of 20 °C to 50 °C and a T_0 of 82.4 K from 60 °C to 95 °C due to mode competition. This value is even larger than that of FP lasers that we achieved before [11], while the FP laser have better heat dissipation. The state-of-art O-band quantum dash and QD micro-lasers achieved T_0 of ~39 K and ~35 K, respectively [19,27]. The extracted T_0 with only SiO_2 passivation was 88.7 K (20 °C to 50°C) and 47.3 K at elevated temperatures. Figure 8(c) presents the red shift of wavelengths with the increase of pump power due to laser self-heating. The slope of dissipated electric power was 0.0235 nm/mW and 0.0378 nm/mW for MRL with and without Al_2O_3 layer before SiO_2, respectively. With increasing temperature, the lasing peak at a fixed injection current, red shifts by ~0.39 nm/°C (Al_2O_3 and SiO_2 passivation) and ~0.34 nm/°C (only SiO_2 passivation), respectively. This shifting is related to the temperature dependence of the refractive index. Thermal impedance of the device was calculated to be 60.6 °C/W and 110.8 °C/W, accordingly. These values of devices with ALD and PECVD layer, are somewhat lower than those of QD lasers [19,28].

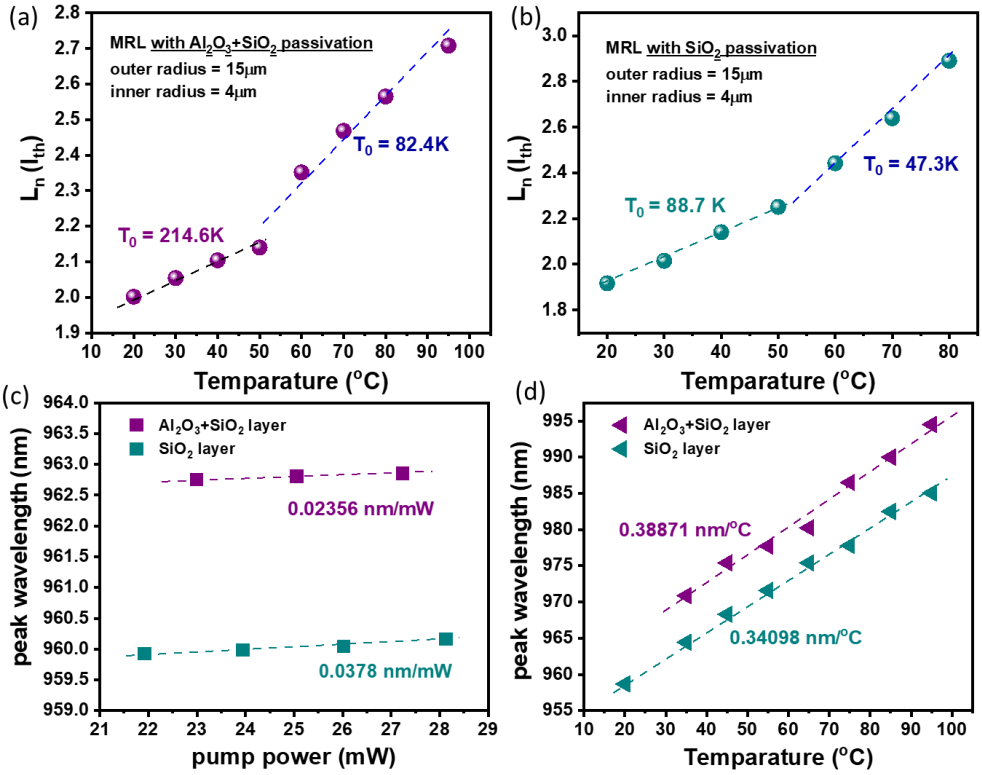

Figure 8. Characteristic temperature of electrically pumped QW MRL (a) with Al_2O_3 + SiO_2 passivation and (b) only SiO_2 passivation; Lasing wavelength as a function of (c) pump power and (d) injection current for the primary lasing modes of the MRL.

The reliability of GaAs-based lasers is of importance for practical applications. The degradation is well-known, primarily related to the defect's formation and propagation during operation and storage [29-31]. The adoption of ALD passivation can provide protection to the facets and address sidewall issues after etching. Figure. 9(a) presents the repeatability of the 25 μm-radius lasers with Al_2O_3 and SiO_2 passivation, with identical threshold and comparable output power (2.86 μW and 2.94 μW). The 20 μm-radius MRL achieved high detected power of 19 μW measured right after the fabrication, as shown in Fig. 9(b). After multiple measurements and six-month storage in the dryer, the MRL shows comparable threshold and slope efficiency, but slightly degraded saturation power which might be due to the optimization of the collection fiber position. The comparable lasing behavior after a long time illustrates that the ALD layer in the passivation could also address the degradation issues of GaAs-based lasers [32-33].

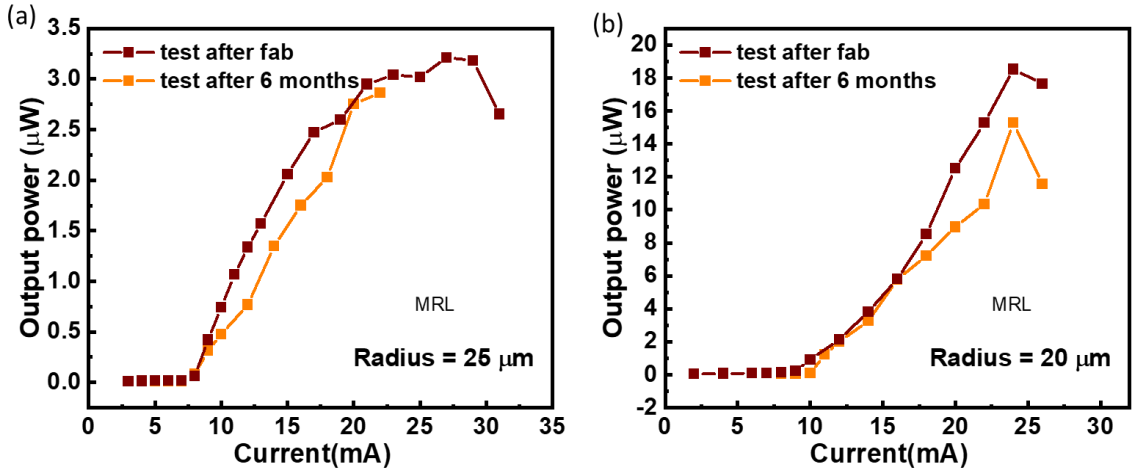

Figure 9. L-I curves of different sweeps (after fabrication and 6 months after fabrication) of MRLs with (a) 25 μm radius and (b) 20 μm-radius, respectively.

Based on the investigation of lasers structures (MRL, MDRM and MDL) and passivation techniques, we fabricated the MDRMs with Al_2O_3 and SiO_2 passivation on the as-grown sample on GaAs/Si template [11], to achieve a low threshold and high reliability. The as-grown epi on GaAs/Si template has gone through around 16-month storage and the related degradation could be observed. However, as shown in Fig. 10(a), the MDRM with 50 μm-radius demonstrates a low threshold current density of ~1.16 kA/cm^2. This value is comparable with the 980 nm FP lasers grown on Si fabricated right after the sample growth [11], although the dimension is smaller and radiation and scattering loss is increased as the WGMs are confined close to the resonator sidewall. Meanwhile, the reported QD micro-lasers on Si achieved a threshold of ~ 5.3 kA/cm^2 [34]. The free spectral range (FSR) was calculated for the fundamental transverse mode using the formula of $\Delta\lambda \approx \lambda^2 / 2\pi R n_g$, wherein n_g is the group refractive index of the cavity, R is the disk radius, and λ represents the emission wavelength. The calculated FSR of 0.88 nm agrees well with the measured FSR of ~0.81 nm. Figure 10 (c) displays the RT emission spectra with progressively increasing current. The transition from spontaneous emission to lasing at 979.4 nm is proved by the sudden narrowing of the emission envelope when the injection current is above the threshold.

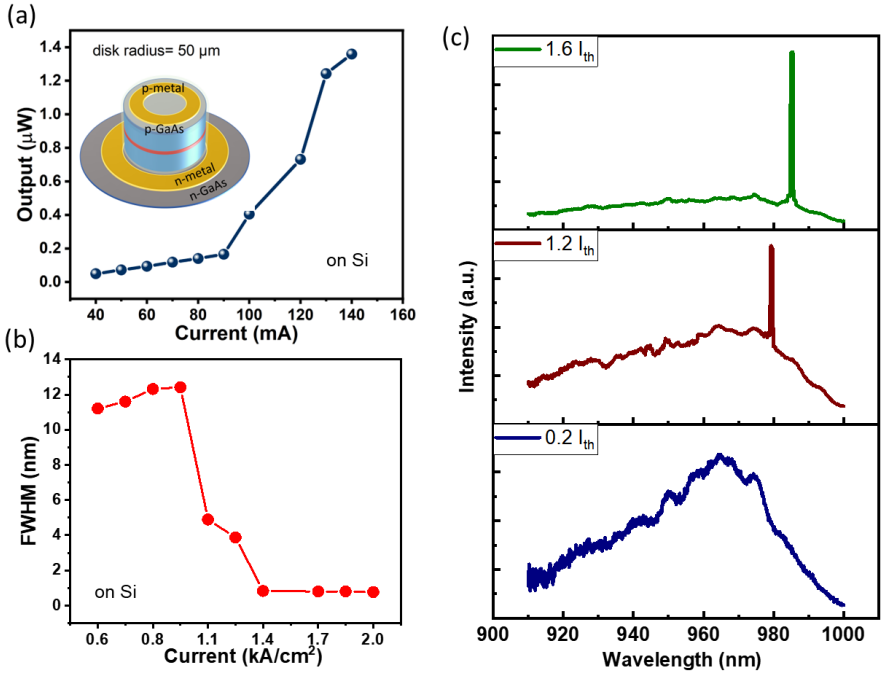

Figure 10. (a) Representative L-I curves of QW MDRM on Si substrate with 50 μm radius in CW mode; (b) corresponding linewidth reduction with increasing pump current; (c) Emission spectra at progressively increased currents of the laser at 20 °C.

IV. Conclusion

In conclusion, to gain some insight on the device design towards lower threshold and minimized power consumption, we demonstrated and compared characteristics of electrically pumped 980 nm QW lasers with various micro-laser cavity structures and passivation layers. The micro-disk lasers with ring-shape metal (MDRM), which were fabricated using a simplified process, demonstrated significantly lower thresholds, higher output power, and improved thermal stability. These benefits can be attributed to reduced non-radiative recombination at the sidewalls and better overlap of the optical fields with carrier injection, resulting in enhanced optical confinement. Furthermore, micro-lasers with ALD passivation exhibited lower lasing thresholds and improved thermal stability. These improvements were achieved through enhanced internal reflection of the resonator and reduced sensitivity to surface recombination. The incorporation of MDRMs and ALD passivation led to the lowest CW threshold of 2.4 mA, sub-milliampere threshold in pulsed mode, a high operating temperature above 95 °C, and a high stability in CW mode. In addition, these optimizations are applied on the lasers grown on GaAs/Si templates leading to a low threshold current density of 1.16 kA/cm^2. All these results represent an advance towards reliable GaAs-based QW micro-lasers to enable dense integration of PICs for a variety of applications including optical communication and internet protocol networks.

Funding. Hong Kong Research Grants Council, University Grants Committee (Grant Nos. 16213420, 16310824, 14212223, and CRS_HKUST404/23); Innovation and Technology Fund (Grant Nos. ITS/201/19FP, ITS/226/21FP).

Acknowledgment

The authors would like to thank Nanosystem Fabrication Facility (NFF) and the Material Characterization &

Preparation Facility (MCPF) of HKUST for their technical support.

Disclosures. The authors declare no conflicts of interest.

Data availability. Data underlying the results presented in this paper are not publicly available at this time but may be obtained from the authors upon reasonable request.

REFERENCES

1. L. Thyl´en, S. He, L. Wosinski, and D. Dai, "The Moore's law for photonic integrated circuits," Journal of Zhejiang University-SCIENCE A, vol. 7, pp. 1961–1967, 2006.
2. M. Smit, J. Van der Tol, and M. Hill, "Moore's law in photonics," pp. 1–13, 2012.
3. E. Stock, F. Albert, C. Hopfmann, M. Lermer, C. Schneider, S. H¨ofling, A. Forchel, M. Kamp, and S. Reitzenstein, "On-chip quantum optics with quantum dot microcavities." Advanced Materials (Deerfield Beach, Fla.), vol. 25, no. 5, pp. 707–710, 2012.
4. T. Zhou, G. Xiang, X. Fang, B. Xiang, X. Liu, S. Hark, and Z. Zhang, "Cantilever-based freestanding InGaP/InGaAlP quantum wells microring lasers," Applied Physics Letters, vol. 114, no. 7, 2019.
5. Z. Yao, K. Wu, B. X. Tan, J. Wang, Y. Li, Y. Zhang, and A. W. Poon, "Integrated silicon photonic micro resonators: emerging technologies," IEEE Journal of Selected Topics in Quantum Electronics, vol. 24, no. 6, pp. 1–24, 2018.
6. Q. Guo, J. Zhang, C. Ning, N. Zhuo, S. Zhai, J. Liu, L. Wang, S. Liu, Z. Jia, and F. Liu, "Continuous-wave operation of microcavity quantum cascade lasers in whispering-gallery mode," ACS Photonics, vol. 9, no. 4, pp. 1172–1179, 2022.
7. W. W. Wong, C. Jagadish, and H. H. Tan, "III–V semiconductor whispering-gallery mode micro-cavity lasers: Advances and prospects," IEEE Journal of Quantum Electronics, vol. 58, no. 4, pp. 1–18, 2022.
8. E. I. Moiseev, M. Maximov, N. V. Kryzhanovskaya, O. I. Simchuk, M. M. Kulagina, S. A. Kadinskaya, M. Guina, and A. E. Zhukov, "Comparative analysis of injection microdisk lasers based on InGaAsN quantum wells and InAs/InGaAs quantum dots," Semiconductors, vol. 54, pp. 263–267, 2020.
9. Y. Xue, W. Luo, S. Zhu, L. Lin, B. Shi, and K. M. Lau, "1.55 μm electrically pumped continuous wave lasing of quantum dash lasers grown on silicon," Optics Express, vol. 28, no. 12, pp. 18 172–18 179, 2020.
10. S. Hu, S. Corzine, K.-K. Law, D. Young, A. Gossard, L. Coldren, and J. Merz, "Lateral carrier diffusion and surface recombination in InGaAs/AlGaAs quantum-well ridge-waveguide lasers," Journal of Applied Physics, vol. 76, no. 8, pp. 4479–4487, 1994.
11. Q. Lin, J. Huang, L. Lin, W. Luo, W. Gu, and K. M. Lau, "980 nm electrically pumped continuous lasing of QW lasers grown on silicon," Optics Express, vol. 31, no. 10, pp. 15 326–15 333, 2023.
12. J. Huang, Q. Lin, W. Luo, W. Gu, L. Lin, and K. M. Lau, "Comparison of quantum well structures for room temperature continuous wave 980 nm lasers grown on (001) Si by MOCVD," Applied Physics Letters, vol. 123, no. 26, 2023.
13. N. Kryzhanovskaya, A. Zhukov, E. Moiseev, and M. Maximov, "III-V microdisk/microring resonators and injection microlasers," Journal of Physics D: Applied Physics, vol. 54, no. 45, p. 453001, 2021.
14. Q. Lin, J. Huang, Y. Xue, L. Lin, Z. Xing, K. S. Wong, and K. M. Lau, "GaAs Microdisk Lasers with Al2O3 Passivation Selectively Grown on SOI", ACS Photonics vol. 11, no. 9, pp. 3578−3584, 2024.
15. N. V. Nguyen, O. A. Kirillov, W. Jiang, W. Wang, J. S. Suehle, P. Ye, Y. Xuan, N. Goel, K.-W. Choi, W. Tsai et al., "Band offsets of atomic-layer-deposited Al_2O_3 on GaAs and the effects of surface treatment," Applied Physics Letters, vol. 93, no. 8, 2008.
16. M. Huang, Y. Chang, C. Chang, Y. Lee, P. Chang, J. Kwo, T. Wu, and M. Hong, "Surface passivation of III-V compound semiconductors using atomic-layer-deposition-grown Al_2O_3," Applied Physics Letters, vol. 87, no. 25, 2005.
17. D. Liang, M. Fiorentino, S. Srinivasan, J. E. Bowers, and R. G. Beausoleil, "Low threshold electrically-pumped hybrid silicon microring lasers," IEEE Journal of Selected Topics in Quantum Electronics, vol. 17, no. 6, pp. 1528–1533, 2011.
18. J. Sass, K. Mazur, F. Eichhorn, W. Strupi´nski, A. Turos, and N. Schell, "Determination of in concentration in InGaAs/GaAs 001 epilayers in the early stage of anisotropic stress relaxation," Journal of alloys and compounds, vol. 401, no. 1-2, pp. 249–253, 2005.
19. Y. Wan, D. Jung, C. Shang, N. Collins, I. MacFarlane, J. Norman, M. Dumont, A. C. Gossard, and J. E. Bowers, "Low-threshold continuous-wave operation of electrically pumped 1.55 μm InAs quantum dash microring lasers," ACS Photonics, vol. 6, no. 2, pp. 279–285, 2018.
20. A. Zhukov, N. Kryzhanovskaya, E. Moiseev, and M. Maximov, " Quantum-dot microlasers based on whispering gallery mode resonators," Light: Science & Applications, vol. 10, no. 1, p. 80, 2021.
21. N. Kryzhanovskaya, E. Moiseev, F. Zubov, A. Mozharov, M. Maximov, N. Kalyuzhnyy, S. Mintairov, Y. A. Guseva, M. Kulagina, S. Blokhin et al., "Evaluation of energy-to-data ratio of quantum-dot microdisk lasers under direct modulation," Journal of Applied Physics, vol. 126, no. 6, 2019.
22. E. I. Moiseev, M. Maximov, N. V. Kryzhanovskaya, O. I. Simchuk, M. M. Kulagina, S. A. Kadinskaya, M. Guina, and A. E. Zhukov, " Comparative analysis of injection microdisk lasers based on InGaAsN quantum wells and InAs/InGaAs quantum dots," Semiconductors, vol. 54, pp. 263–267, 2020.
23. A. Fiore, M. Rossetti, B. Alloing, C. Paranthoen, J. Chen, L. Geelhaar, and H. Riechert, "Carrier diffusion in low-dimensional semiconductors: A comparison of quantum wells, disordered quantum wells, and quantum dots," Physical Review B, vol. 70, no. 20, p. 205311, 2004.
24. H. J. Joyce, C. J. Docherty, Q. Gao, H. H. Tan, C. Jagadish, J. Lloyd Hughes, L. M. Herz, and M. B. Johnston, "Electronic properties of GaAs, InAs and InP nanowires studied by terahertz spectroscopy," Nanotechnology, vol. 24, no. 21, p. 214006, 2013.
25. M. Bosund, P. Mattila, A. Aierken, T. Hakkarainen, H. Koskenvaara, M. Sopanen, V.-M. Airaksinen, and H. Lipsanen, "GaAs surface passivation by plasma-enhanced atomic-layer-deposited aluminum nitride," Applied Surface Science, vol. 256, no. 24, pp. 7434–7437, 2010.
26. P. D. Ye, G. D. Wilk, J. Kwo, B. Yang, H. J. Gossmann, M. Frei, S.N.G. Chu, J.P. Mannaerts, M. Sergent, M. Hong, K. K. Ng and J. Bude, "GaAs MOSFET with oxide gate dielectric grown by atomic layer deposition". IEEE Electron Device Letters, vol. 24, no. 4, pp. 209-211, 2003.
27. Y. Wan, D. Jung, J. Norman, C. Shang, I. MacFarlane, Q. Li, M. Kennedy, A. C. Gossard, K. M. Lau, and J. E. Bowers, "O-band electrically injected quantum dot micro-ring lasers on on-axis (001) GaP/Si and V-groove Si," Optics express, vol. 25, no. 22, pp. 26 853–26 860, 2017.
28. E. Moiseev, N. Kryzhanovskaya, M. Maximov, F. Zubov, A. Nadtochiy, M. Kulagina, Y. Zadiranov, N. Kalyuzhnyy, S. Mintairov, and A. Zhukov, "Highly efficient injection microdisk lasers based on quantum well-dots," Optics Letters, vol. 43, no. 19, pp. 4554–4557, 2018.
29. R. V. Ghita, M. F. Lazarescu, A. S. Manea, C. Logofatu, E. Vasile, and V. Ciupina, "Facet oxidation and degradation of AlGaAs/GaAs pulsed laser diodes," in ROMOPTO 2003: Seventh Conference on Optics, vol. 5581. SPIE, 2004, pp. 268–273.
30. Y. Sin, Z. Lingley, M. Brodie, B. Knipfer, C. Sigler, C. Boyle, J. Kirch, K. Oresick, H. Kim, D. Botez et al., "Catastrophic degradation in high-power buried heterostructure quantum cascade lasers," in CLEO: Science and Innovations. Optica Publishing Group, 2019, pp. SW3N–3.
31. F. Nash, R. Hartman, N. Denkin, and R. Dixon, "GaAs laser reliability and protective facet coatings," Journal of Applied Physics, vol. 50, no. 5, pp. 3122–3132, 1979.
32. S. Yellen, A. Shepard, R. Dalby, J. Baumann, H. Serreze, T. Guido, R. Soltz, K. Bystrom, C. Harding, and R. Waters, "Reliability of GaAs-based semiconductor diode lasers: 0.6-1.1 μm," IEEE journal of quantum electronics, vol. 29, no. 6, pp. 2058–2067, 1993.
33. C. Hanke, L. Korte, B. D. Acklin, J. Luft, S. Groetsch, G. Herrmann, Z. Spika, M. Marchiano, B. DeOdorico, and J. Wilhelmi, "Highly reliable 40w CW InGaAlAs/GaAs 808-nm laser bars," in In-Plane Semiconductor Lasers III, vol. 3628. SPIE, 1999, pp. 64–70.
34. S. Zhu, B. Shi, and K. M. Lau, "Electrically pumped 1.5 μm InP-based quantum dot microring lasers directly grown on (001) Si," Optics letters, vol. 44, no. 18, pp. 4566–4569, 2019.

Qi LIN received the Ph.D. degree from the Hong Kong University of Science and Technology, Hong Kong, in 2024. She is currently a Postdoctoral Research Associate with the Department of Electrical and Computer Engineering, University of Virginia. Her research interests include III-V lasers and avalanche photodetector.

Ying Xue received the Ph.D. degree from the Department of Electrical and Computer Engineering, Hong Kong University of Science and Technology, in 2022. She is currently a Research Assistant Professor in Division of Emerging Interdisciplinary Areas, Hong Kong University of Science and Technology. Her research interest has been in the area of III-V optoelectronic devices and their integration with silicon photonics.

Jie Huang received the Ph.D. degree from the Department of Electrical and Computer Engineering, Hong Kong University of Science and Technology, in 2023. He was a Postdoctoral Research Associate with the Hong Kong University of Science and Technology. His research focuses on III-V epitaxy by MOCVD.

Wen Gu received the Master degree in Institute of Semiconductors, Chinese Academy of Sciences, China. He is currently working toward the Ph.D. degree with Hong Kong University of Science and Technology. His research interests include growth and characterization of III-V quantum dot laser epitaxially grown on silicon.

Kei May Lau received her degrees from the University of Minnesota and Rice University and served as a faculty member at the University of Massachusetts/Amherst before joining HKUST in the summer of 2000. She is an elected member of the US National Academy of Engineering, a Fellow of IEEE, Optica (formerly OSA), and the Hong Kong Academy of Engineering. She was also a recipient of the IPRM award, IET J J Thomson medal for Electronics, Optica Nick Holonyak Jr. Award, IEEE Photonics Society Aron Kressel Award, US National Science Foundation (NSF) Faculty Awards for Women (FAW) Scientists and Engineers, and Hong Kong Croucher Senior Research Fellowship. She is a Fellow of the OSA (2019), a recipient of the U.S. National Science Foundation (NSF) Faculty Awards for Women (FAW) Scientists and Engineers (1991), Croucher Senior Research Fellowship (2008), and the IEEE Photonics Society Aron Kressel Award (2017). She was an Editor of the IEEE Transactions on Electron Devices and Electron Device Letters, an Associate Editor for the Journal of Crystal Growth and Applied Physics Letters. Lau's research work focuses on the development of monolithic integration of semiconductor devices and systems on industry-standard silicon substrates by MOCVD. She was an early explorer of this approach and has produced record-breaking results in this area.